EurJOC
European Journal of Organic Chemistry

A Journal of
ChemPubSoc Europe

# Accepted Article

**Title:** Synthesis of Thiazoles Bearing Aryl Enamine/Aza-enamine Side Chains. Effect of the π-Conjugated Spacer Structure and Hydrogen Bonding on Photophysical Properties

**Authors:** Kseniya I. Lugovik, Aleksandra V. Popova, Alexander K. Eltyshev, Enrico Benassi, and Nataliya Belskaya



**To be cited as:** *Eur. J. Org. Chem.* 10.1002/ejoc.201700518

**Link to VoR:** http://dx.doi.org/10.1002/ejoc.201700518

**Supported by**
ACES Asian Chemical Editorial Society

WILEY-VCH

10.1002/ejoc.201700518

WILEY-VCH

FULL PAPER

# Synthesis of Thiazoles Bearing Aryl Enamine/Aza-enamine Side Chains. Effect of the π-Conjugated Spacer Structure and Hydrogen Bonding on Photophysical Properties

Kseniya I. Lugovik,[a] Aleksandra V. Popova,[a] Alexander K. Eltyshev,[a] Enrico Benassi,*[b] Nataliya P. Belskaya*[a]

**Abstract:** An efficient synthesis of a new series of di- and trisubstituted thiazoles (**TZ**s) bearing aryl enamine side chains (**ETZ**s) was developed, and the optical properties of these compounds were compared with structural analogues containing the isoelectronic aza-enamine group (**ATZ**s). Spectral characterization has demonstrated the difference in the absorption and fluorescence of the **ETZ**s and **ATZs** in solution and emergence of fluorescence **ETZ**s in a solid state. The optimized structural geometries and weak intramolecular interactions, electronic characteristics of the ground and excited states, HOMO and LUMO analysis, changes in electron density after the $S_0 \rightarrow S_{1v}$ excitation, and map of the electrostatic potential (MEP) calculated at DFT level allowed us to estimate the particularities in the geometric and electronic structures of the **ETZ**s and **ATZ**s in the ground and excited states. The availability, synthetic simplicity, stability, large Stokes shift, and high sensitivity to the microenvironment (fluorosolvatochromic behaviour) make the obtained **TZ**s a useful platform for the further design and synthesis of new effective compounds for applications in the field of fluorescence imaging.

## Introduction

Thiazoles and their derivatives are abundant in natural products, biologically active compounds and some pharmaceuticals.[1] This structural element is also found in commercial products, such as thiazole orange, which is a commonly used cyanine dye for binding to nucleic acids. In this compound, the thiazole ring is part of a benzothiazole, which is especially suitable for biosensors and imaging applications.[2] Substituted monocyclic thiazoles (**TZ**s), which are typically linked to aryl or heteroaryl groups, are privileged structural motifs applied in different fields, such as materials science, for the preparation of liquid crystals, molecular switches, and sensors.[3] Furthermore, because of the low toxicity of the derivatives of this heterocycle, the thiazole moiety continues to be a key pharmacophore for medicinal chemistry and drug discovery research.[4] Thus, the various applications of thiazoles allow them to remain a focus in heterocyclic chemistry.

A remarkable advantage for the development of new synthetic thiazole is the numerous convenient methods for their construction, which give different possibilities for peripheral derivatization [5] and allow the tuning of the optical properties of these compounds by varying their electronic nature with electron-donor and electron-acceptor groups and the length and nature of their conjugated systems. The most well-known approach for forming the thiazole ring is the Hantzsch synthesis, where primary thioamides or thioureas react with α-halocarbonyl compounds to afford various **TZ**s in a single step.[5,6] This is an excellent method for functionalizing thiazole rings with primary, secondary and tertiary amine groups and different electron-donating and electron-accepting alkyl, aryl, and heteroaryl substituents.[3]

An eloquent example of the excellent fluorescence of this heterocycle derivatives depending on the attached substituents structure is represented by recently published results of the synthesis and investigation of photophysical properties for a series of 5-arylaminothiazoles, with wide tuned emission ranged from 460 to 610 nm and fluorescence quantum yield between 0.01-0.86.[3d] A family of asymmetrical D-π-A and symmetrical D-π-D types of thiazole-based fluorescent compounds were prepared also and their photophysical and electrochemical characteristics exhibit high electrochemical activity with a green fluorescence emission.[3e] 4-Hydroxy-1,3-thiazoles were suggested as a new class of promising functional fluorophores and therefore they are extensively studied for various application.[3c] The azide-modified thiazole-based reporter molecule with better properties for fluorescence and UV detection compare to the commercially available fluorophores were also synthesized and characterised.[3f]

On the other hand, introducing flexible bridge within the molecule increases the ability of these compounds to adopt various structural conformations and form weak intra/intermolecular interactions that may affect the chemical, photophysical and biological properties and may be used to control them.[7] Thus, estimating the relationships between the structural features and the ratios of conformers/rotamers and intra/intermolecular hydrogen bonding is essential for different applications. To understand the fluorescence of a molecule, it is important to know its conformational properties, which may help to predict the energy irradiation during vibrational relaxation. Hence, weak interactions are notable and may play a central role, because they affect the energy of the oscillations of a molecule's excited states and probability of its vibrational transitions.

The most commonly employed and widely studied flexible bridging structures linking the donor and acceptor moieties of the photoactive molecule are polymethine chain, ethylene, azo or azomethine bonds.[8] We propose to study structural features and photophysical properties of compounds **1** and **2** (Figure 1), which

[a] Kseniya, I. Lugovik, Aleksandra V. Popova, Alexander K. Eltyshev, Prof. Nataliya P. Belskaya
Ural Federal University
19 Mira Str., Yekaterinburg 620002 (Russian Federation)
E-mail: n.p.belskaya@urfu.ru

[b] Dr. Enrico Benassi
Scuola Normale Superiore,
Piazza dei Cavalieri 7 56126, Pisa (Italy)
E-mail: enrico.benassi@sns.it

Supporting information for this article is given via a link at the end of the document.

bear a conjugated π-spacer, including -NH-X=C< link, and differ from each other only by a CH unit (in compound **1**) replaced by a N atom (in compound **2**). Moreover, compounds **1** and **2** are suitable for formation of possible intramolecular hydrogen bonds due to the presence of the NH-fragment and thiazole nitrogen atom as donor of electrons.

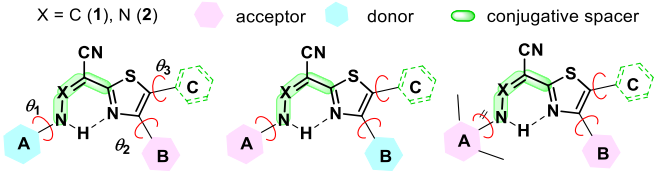


**Figure 1.** Design of the new thiazole derivatives with aryl enamine and aryl aza-enamine side groups.

A convenient method for the synthesis of azaenaminethiazoles (**ATZs**) was described in the literature and is based on the reaction of arylhydrazonothioacetamides with bromoacetophenones.[6] However, at the best of our knowledge, there are no reported examples of synthesis of thiazoles using thioamides bearing enamine functional groups. This may be explained by the unique reactivity of enamino group, which usually produces thiophenes by reacting with haloketones.[9] The development of a simple protocol for thiazole synthesis based on broad pool of potential starting reagents provides prospects for the synthesis of a set desired compounds with different types of the push-pull systems (Figure 1).

The main goal of our investigation is, therefore, to design and synthesize thiazoles **1** with an aryl enamine side group (X=C) and compare their electronic characteristics, fine structures, weak intramolecular interactions and photophysical properties to those of their structural analogous – aza-enamines **2** (X=N) – using experimental and theoretical methods (Figure 1). The structures of compounds **1** and **2** involve an aryl(**B**)/diaryl(**B**,**C**)-substituted heterocyclic ring and an additional aromatic/heteroaromatic cycle (**A**) with electron-donating and electron-accepting groups, which are interlinked by a conjugated system.

The dependency of the electronics, location and strength on the substituents on opposite sides of the molecules allows us to evaluate the effect of the enamine/aza-enamine chains on intramolecular charge transfer (ICT), photophysical properties and weak intramolecular interactions.

## Results and Discussion

### Synthesis and characterization

The required starting materials for the synthesis of thiazoles **1** are arylaminothioacrylamides **6** with unsubstituted thioamide group. For their synthesis, we apply a recently developed protocol based on the condensation of cyanothioacetamide **3** with dimethylformamide dimethyl acetal (DMFDMA), followed by the nucleophilic substitution of the dimethylamine moiety with the desired arylamines **5a-f**,**h** and 9-ethyl-aminocarbazole (**5g**) (Scheme 1, Table 1).[10]

A variety of substituents was introduced to the 4- and 2-positions of the arylamino moiety in enamines **6a-h** using arylamines **5a-h**. The reactions of 3-amino-9-ethylcarbazole (**5g**) and *N*-methyl-*N*-phenylamine (**5h**) also afforded compounds **6g,h** with good yields.

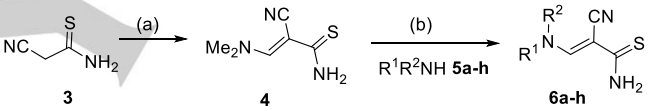


**Scheme 1.** Reagents and conditions: (a) Dimethylformamide dimethylacetale, EtOH, 50 °C, 5h; (b) $R^1R^2NH$ (**5a-h**) EtOH, HCl, 60 °C.

The structures of arylaminothioacrylamides **6** were confirmed by FTIR, $^1$H NMR, $^{13}$C NMR, mass spectrometry and elemental analysis data. Details of the experimental procedures and data for the structural characterization are disclosed in the Experimental Section and Supporting Information (SI). Notably, the NMR spectra show that compounds **6a-g** exist as a mixture of two steric isomers (SI, Figures S1-8).

**Table 1.** Conversion time of thioamide **4** in its reactions with arylamines **5a-h**, yields of arylaminothioacrylamides **6a-h**, and ratios of isomers.

| Entry | Comp **5** | $R^1$ | $R^2$ | Comp **6** | $R^1$ | $R^2$ | Ratio of isomers **6**[a] | Time [h] | Yield **6** [%][b] |
|---|---|---|---|---|---|---|---|---|---|
| 1 | **5a** | 4-$MeOC_6H_4$ | H | **6a** | 4-$MeOC_6H_4$ | H | 1:2 | 2.0 | 89 |
| 2 | **5b** | Ph | H | **6b** | Ph | H | 2:5 | 4.0 | 56 |
| 3 | **5c** | 4-$ClC_6H_4$ | H | **6c** | 4-$ClC_6H_4$ | H | 1:4 | 4.0 | 80 |
| 4 | **5d** | 4-$O_2NC_6H_4$ | H | **6d** | 4-$O_2NC_6H_4$ | H | 1:4 | 5.0 | 99 |
| 5 | **5e** | 2-$ClC_6H_4$ | H | **6e** | 2-$ClC_6H_4$ | H | 1:9 | 8.0 | 82 |
| 6 | **5f** | 2,6-$Cl_2C_6H_3$ | H | **6f** | 2,6-$Cl_2C_6H_3$ | H | 1:2 | 8.0 | 60 |
| 7 | **5g** | 9-Ethylcarbazol-3-yl | H | **6g** | 9-Ethylcarbazol-3-yl | H | 2:3 | 2.0 | 75 |
| 8 | **5h** | Ph | Me | **6h** | Ph | Me | -[c] | 4.5 | 70 |

[a] The isomeric ratio was determined from the $^1$H NMR spectra in DMSO-$d_6$. [b] Isolated yield. [c] One set of signals in $^1$H NMR spectrum.

For the synthesis of **ETZ**s **1**, the Hantzsch reaction was performed according to the protocol previously used for the interaction of arylhydrazonothioacetamides with halocarbonyl compounds.[6] Screening the conditions for the reaction of arylaminothioacrylamide **6a** with phenacyl bromide **7a** (DMF, TEA, 80 °C and DMF, 80 °C) demonstrated that the reaction proceeds well without any base and selectively lead to formation only one product (**1a**) (Scheme 2, Table 2). Further reactions of bromoacetophenones **7a**,**b** and 2-chloro-1,2-diphenylethanone **7c** with thioamides **6a-h** under moderate heating in DMF produced **ETZ**s **1a-j** in good yields (Table 2).

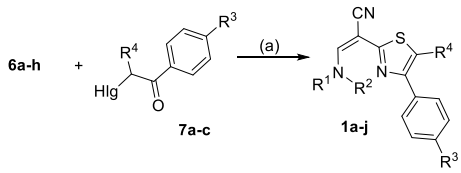


| 7 | $R^3$ | $R^4$ | Hlg |
|---|---|---|---|
| a | Cl | H | Br |
| b | $NO_2$ | H | Br |
| c | H | Ph | Cl |

**Scheme 2.** Reagents and conditions: (a) DMF, 80 °C, 0.5-2h.

Products **1a-j** were fully characterized using spectroscopic analysis: FTIR, $^1$H NMR, $^{13}$C NMR (see the Experimental Section and SI, Figures S9-19), and EI-MS, and their purity was established using elemental analysis. In the IR spectra, the characteristic bands for the stretching vibrations of C≡N and N-H bonds were observed at 2199-2210 cm$^{-1}$ and at 3101-3256 cm$^{-1}$, respectively. The mass spectra of **ETZ**s **1a-j** each exhibited a molecular ion with high intensity (approximately 100%).

The $^1$H NMR spectra of thiazoles **1a-d**,**g** exhibited two sets of signals, while compounds **1e**,**f**,**h-j** displayed one set of signals. The most noteworthy signals were the doublet (or doublets) of the CH-enamine moiety, and signals of the protons of the aromatic rings (**A**, **B** and **C**) and proton-containing substituents in the **A**- and **B**-cycles and for compounds **1a-h**,**g** ($R^4$ = H) the singlet or two singlets of the C5H-thiazole proton at 7.7-8.5 ppm.

The advantage of this method is the possibility of introduce two aromatic cycles on the thiazole ring simultaneously, which was achieved in the condensation of 2-chloro-1,2-diphenylethanone (**7c**). It should be mentioned that usually, transition-metal-catalysed coupling reactions for forming new C-C bonds are applied for this type of extension of the π–conjugated system of a molecule.[10] This well-known and widespread strategy requires expensive catalysts, solvents, and reagents and elongate the process by requiring additional stages, i.e., halogenation of the thiazole ring followed by a palladium-catalysed cross-coupling reaction with an aryl boronate ester.

**Table 2.** Conversion time of thioamides **6a-h** in their reactions with 2-bromoacethophenones **7a**,**b**, and 2-chloro-1,2-diphenylethanone (**7c**), yields of **ETZ**s **1a-j**, and the ratios of the isomers of thiazoles **1a-j**.

| Entry | Comp **1** | $R^1$ | $R^2$ | $R^3$ | $R^4$ | Ratio of isomers **6**[a] | Time [h] | Yield **6** [%][b] |
|---|---|---|---|---|---|---|---|---|
| 1 | **1a** | 4-$MeOC_6H_4$ | H | Cl | H | 9:1 | 1.5 | 65 |
| 2 | **1b** | Ph | H | Cl | H | 10:1 | 2.0 | 84 |
| 3 | **1c** | 4-$ClC_6H_4$ | H | Cl | H | 6:1 | 1.0 | 80 |
| 4 | **1d** | 4-$O_2NC_6H_4$ | H | Cl | H | 4:1 | 1.0 | 74 |
| 5 | **1e** | 2-$ClC_6H_4$ | H | Cl | H | -[c] | 3.0 | 83 |
| 6 | **1f** | 2,6-$Cl_2C_6H_3$ | H | Cl | H | -[c] | 1.0 | 80 |
| 7 | **1g** | 4-$MeOC_6H_4$ | H | $NO_2$ | H | 7:1 | 0.5 | 67 |
| 8 | **1h** | 9-Ethylcarbazol-3-yl | H | Cl | H | -[c] | 1.5 | 68 |
| 9 | **1i** | 4-$MeOC_6H_4$ | H | H | Ph | -[c] | 4.0 | 70 |
| 10 | **1j** | Ph | Me | Cl | H | -[c] | 1.5 | 70 |

[a] The isomeric ratio was determined from the $^1$H NMR spectra in DMSO-$d_6$. [b] Isolated yield. [c] One set of signals in $^1$H NMR spectrum.

The analogous thiazoles **2a-d**, which have aza-enamine functionalities (**ATZ**s), were obtained following the same procedure as was depicted in Scheme 2 for enamines **6** (Scheme 3, Table 3). The obtained results demonstrated the differences in the reactivities of these two types of compounds. For example, aza-enamines **8a-c** reacted with halocarbonyls faster than enamines **6a-c**.

The synthesized compounds (**2a-d**) were characterized by elemental analysis, MS, FTIR and NMR. These data, which are detailed in the Experimental Section, are consistent with the proposed structures. Similar to **ETZ**s **1a-d**,**g**, **ATZ**s **2a-d** exhibited two sets of signals in their NMR spectra (Table 3, Figures S20-23).

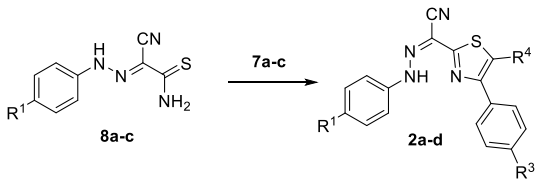


**Scheme 3**. Reagents and conditions: DMF, 80 °C, 0.5-3 h.

**Table 3.** Yields and conversion times for the synthesis of **ATZ**s **2a-d** and ratios of isomers.

| Entry | **ATZ**s | $R^1$ | $R^3$ | $R^4$ | Time [h] | Yield[a] [%] | Ratio of isomers **2**[b] |
|---|---|---|---|---|---|---|---|
| 1 | **2a** | MeO | Cl | H | 0.5 | 64 | 2:3 |
| 2 | **2b** | H | Cl | H | 0.5 | 86 | 1:2 |
| 3 | **2c** | $NO_2$ | Cl | H | 1.0 | 85 | 1:3 |
| 4 | **2d** | MeO | H | Ph | 3.0 | 75 | 1:2 |

[a] Isolated yield. [b] The isomeric ratio was determined from the $^1$H NMR spectra in DMSO-$d_6$.

### Molecular structures of ETZs and ATZs

As mentioned above, most examples of compounds **1** and **2** exist as a mixture of steric isomers (rotamers) because of the different locations of substituents relative to the double bonds (-HC=C< for the enamines and -N=C< for the aza-enamines) and because of the two conjugated double bonds (C=C and endocyclic C=N bonds) in the molecules. The isomeric ratios for compounds **1a** and **2a** are evaluated by quantum mechanical calculations. The optimized structures of the isomers of compounds **1a** and **2a** are shown in Figure 2. The thermochemical results computed in dioxane show that **1a**-*Z*,*Z* and **2a**-*Z*,*Z* are unambiguously the most stable isomers. The second most stable isomers for enamine **1a** and aza-enamine **2a** are **1a**-*E*,*Z*, and **2a**-*E*,*E*, respectively.

The $^1$H NMR spectra of the isomers of **TZ**s **1a** and **2a** were simulated in 1,4-dioxane and chloroform (SI, Table S1-4). The experimental data and quantum mechanical calculation results demonstrate the correlation of the chemical shifts of the proton-containing groups with those of the most stable *Z*,*Z*-rotamer.

Analysis of the optimized geometry of the **TZ**s isomers shows that the preferred formation of the *Z*,*Z*-rotamer can be ascribed to the hydrogen bonding between the NH group of the enamine/aza-enamine and the nitrogen atom of the thiazole ring ($N_{TZ}$). To study the weak bond formation in the structure of **TZ**s, isomers **1a-g**,**i** and **2a**,**c**,**d** were subjected to the standard atoms in molecules (AIM) theory of bonding based on electron density.[11] The BCP (bond critical point) (3, -1)-type for the N1H···$N_{TZ}$ hydrogen bond and RCP (ring critical points) (3, +1) for the pseudo-cycle, which is formed by the NH-enamine/aza-enamine chain and N-atom of the **TS** ring (Figure 3 and additional examples in the SI, Figure S26) confirm hydrogen bond formation in the structures of the *Z*,*Z*-isomers.

However, the AIM theory is not ideal for investigating and visualizing non-covalent interactions (NCIs). The absence of a BCP should not necessarily be considered as evidence of the absence of a chemical bond. Therefore, we additionally apply a recently introduced type of NCI Index[12] as a more general description of intramolecular interactions based on density changes instead of its local values, as was done in the AIM method. The NCI index is defined as a normalized and dimensionless reduced density gradient (RDG),

$$s = \frac{1}{2(3\pi^2)^{1/3}} \frac{|\nabla\rho|}{\rho^{4/3}}.$$

The RDG value demonstrates the probability of NCI formation. The attractive/repulsive character of this interaction can be identified by the sign of the RDG second derivative along the second main axis of variation $\lambda_2$ (eigenvalue), which is negative for attractive interactions and positive for repulsive ones (Figure 4 and SI, Figure S27). This approach has been developed to reveal non-covalent interactions (e.g., hydrogen bonding) in 3D space. Regions where the electron density $\rho$(r) and reduced electron density gradient *s* are low correspond to regions where non-covalent interactions occur. It follows that isosurfaces of the reduced density gradient at low densities can be used to visualize the position and nature of non-covalent interactions in 3D space. NCI isosurfaces, therefore, illustrate the nature of the intramolecular interactions. A continuous color-coding scheme based on the second derivatives is used to provide qualitative information about the strength of interaction, where strong attractive interactions are represented in blue, weak interactions in green, and strong repulsive interactions in red.

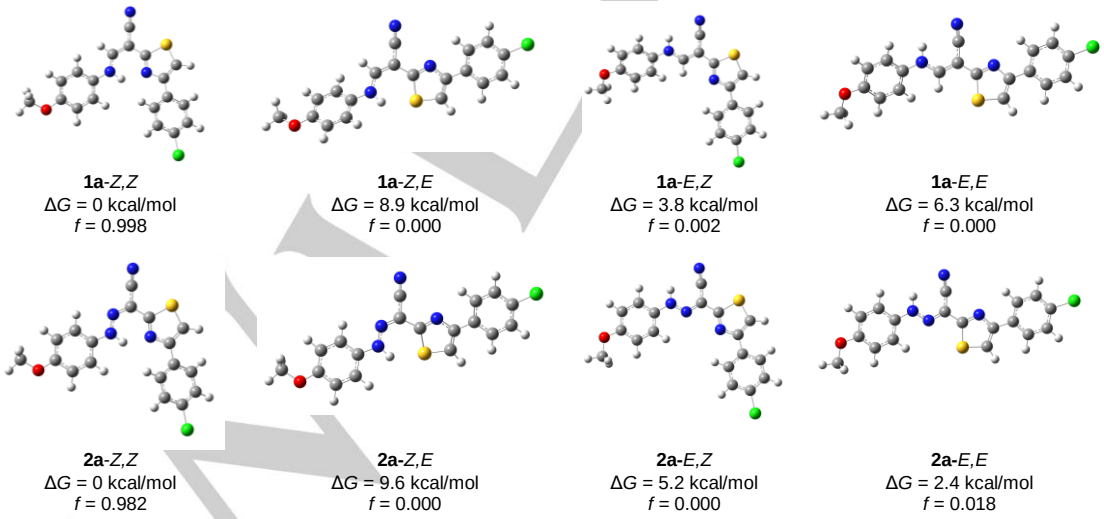


**Figure 2.** Computational results for the relative stability (Δ*G*) of the isomers of **ETZ 1a** and **ATZ 2a**. Level of theory: DFT M06-2X (SMD) / aug-cc-pVTZ. The Boltzmann factors (*f*) at 300 K are also reported.

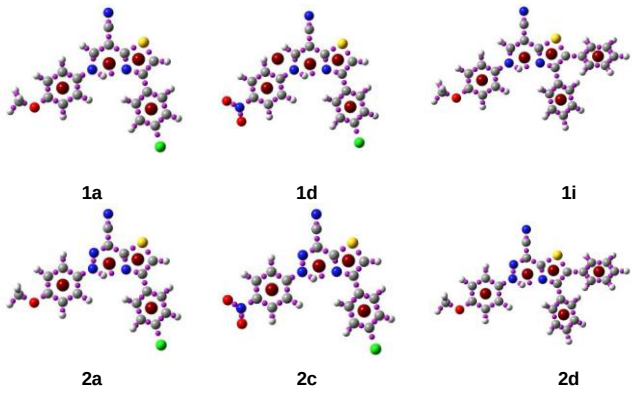


**Figure 3.** Critical points *GS* ($S_0$) for the *Z*,*Z*-isomers of compounds **1a**,**d**,**i**, and **2a**,**c**,**d** in dioxane. Colour legend of the atoms: white (H), grey (C), blue (N), red (O), and yellow (S). Colour legend for CPs: dark-red (RCP) and pink (BCP).

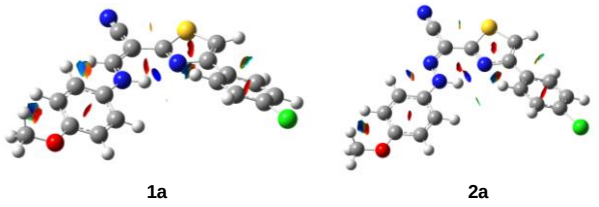


**Figure 4.** Plots of the NCI isosurfaces (*s* = 0.5 a.u. and a blue-green-red colour scale from -0.012 a.u. < sign($\lambda_2$) ρ(r) < +0.012 a.u.) for the *Z*,*Z*-rotamers of compounds **1a** and **2a** in the ground state.

These results provide additional proof of the ability of the weak NH···$N_{TZ}$ interaction to effectively stabilize the *Z*,*Z*-isomers of enamines **1a-i** and aza-enamines **2a-c**. This phenomenon results in the folding of the flexible side chain (enamine or aza-enamine).

## Electronic absorption and fluorescence

The UV–vis spectra of thiazoles **1a**,**b**,**d** and **2a-c** are recorded in ethanol, and their molar absorption coefficients ***ε*** at absorption maxima ($\lambda_{abs}$) are recorded in Table 4. The UV−vis absorption spectra (Figure 5) show maxima in three separate regions: 245-257 nm, 282-298 nm and 373-416 nm. **ETZ 1c**, which has a strong electron-accepting group ($R^1$ = 4-$NO_2$) exhibits an additional band at 535 nm, which is caused by the strengthening of intramolecular charge transfer (ICT) due to the strong interaction of the molecule with the highly polar solvent.[7a] The replacement of the electron-donating substituents with electron-accepting ones in the aromatic portion (**A**) of enamines **1a-c** causes a small redshift (up to 26 nm).

The fluorescence emission profiles of thiazoles **1a-j** and **2a**,**c**,**d** are recorded in dioxane (Figure 6). The absorption ($\lambda_{abs}$) and emission maxima ($\lambda_{em}$), extinction coefficient (***ε***), and quantum yield ($\Phi_F$) of thiazoles **1a-j** and **2a**,**c**,**d** are presented in Table 5. All compounds show a single fluorescence emission band with a maxima between 404 and 515 nm. These bands are more redshifted with respect to the corresponding absorption spectra, which indicates the effect of enhanced conjugation on the singlet state ($S_1$).

**Table 4.** UV spectra[a] of **ETZ**s **1a**,**b**,**d** and **ATZ**s **2a**-**c** in EtOH.

| Entry | Thiazoles **1,2** | $\lambda_{abs}$ [nm] | $\varepsilon_{max}$ [$M^{-1}\cdot cm^{-1}$] |
|---|---|---|---|
| 1 | **1a** | 254, 298, 373 | 36800, 8260, 31241 |
| 2 | **1b** | 249, 292, 367 | 31021, 7618, 25681 |
| 3 | **1d** | 244, 291, 393 | 6880, 2980, 6600 |
| 4 | **2a** | 251, 291, 414 | 26380, 6420, 23320 |
| 5 | **2b** | 245, 286, 397 | 31763, 8278, 25237 |
| 6 | **2c** | 247, 282, 416 | 11228, 6778, 13188 |

[a] UV-vis absorption wavelengths at room temperature ($c$ = 5×$10^{-5}$ mol/L).

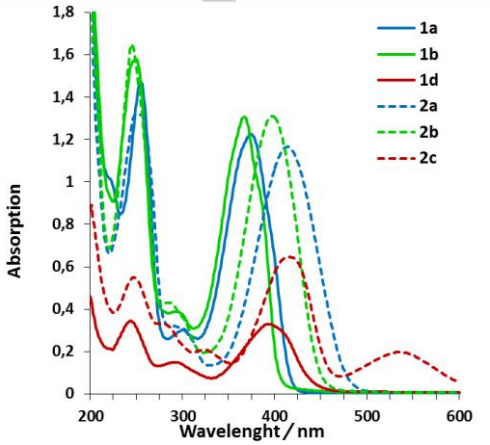


**Figure 5.** Electronic absorption spectra of **ETZ**s **1a**,**b**,**d** and **ATZ**s **2a-c** in EtOH at room temperature ($c$ = 5×$10^{-5}$ mol/L).

The structure of enamines **1a-j** substantially affects their emission characteristics. The largest quantum yields were obtained for compounds **1e-g** (Table 5, entries 5-7). We can assume that this is explained by the limited rotation of the aromatic cycle (**A**) around the σ-bond because of the spatial effect of the substituent or two substituents at the ortho-positions of **ETZ**s **1e** and **1f**.

The strengthening of the rigidity of **ETZ 1g**, which has a push-pull system in its structure, may be the reason for the strong conjugation in molecule as it increases the partial double character of the σ–bonds, restricting the molecular rotation in the *ES*.

The Stokes shifts of the thiazoles are relatively large (35-112 nm) and vary depending on the combination of electronic and spatial effects of the substituents on aromatic cycles (**A** and **B**). **ETZ**s **1d**,**g**, which have substituents on their aromatic rings with the opposite electronic effect, exhibit larger Stokes shift values (Table 5, entries 4,7). **ETZ 1c** with the same substituents in the aromatic cycles (**A** and **B**), and **ETZ**s **1e**,**f**, which have one or two substituents at the ortho-positions in aromatic cycle **A**, show smaller Stokes shifts (Table 5, entries 5 and 6).

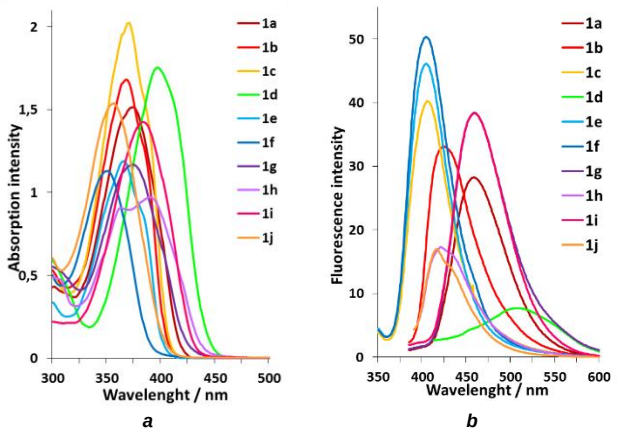


**Figure 6**. Absorption (**a**) and emission (**b**) spectra of **ETZ**s **1a-j** in dioxane at room temperature.

**Table 5.** Photophysical properties of **ETS**s **1a-j** and **ATS**s **2a**,**c**,**d** in dioxane.

| Entry | Comp | $\lambda_{max}$[a] [nm] | $\varepsilon_{max}$ [$M^{-1}$ $cm^{-1}$] | $\lambda_{em}$[b] [nm] | $\Phi_F$[c] [%] | Stokes shift, [nm/$cm^{-1}$] |
|---|---|---|---|---|---|---|
| 1 | **1a** | 374 | 25342 | 458 | 1.15 | 84/4904 |
| 2 | **1b** | 368 | 23688 | 424 | 1.00 | 56/3589 |
| 3 | **1c** | 371 | 34173 | 406 | 0.79 | 35/2324 |
| 4 | **1d** | 397 | 37266 | 509 | 0.43 | 112/5543 |
| 5 | **1e** | 366 | 22115 | 404 | 1.68 | 38/2570 |
| 6 | **1f** | 350 | 25533 | 405 | 2.14 | 55/3880 |
| 7 | **1g** | 374 | 27594 | 459 | 2.05 | 85/4951 |
| 8 | **1h** | 390 | 24274 | 421 | 1.00 | 31/1888 |
| 9 | **1i** | 383 | 26524 | 459 | 1.64 | 76/4323 |
| 10 | **1j** | 357 | 24162 | 416 | 0.50 | 59/3973 |
| 11 | **2a** | 414 | 26627 | 462 | 0.10 | 48/2510 |
| 12 | **2c** | 409 | 43771 | 480 | 0.10 | 71/3617 |
| 13 | **2d** | 423 | 27946 | 515 | 0.05 | 92/4223 |

[a] UV-vis absorption wavelengths at room temperature and a concentration of $c$ = 5×$10^{-5}$ mol/L. [b] Fluorescence wavelengths at room temperature at a concentration of $10^{-6}$ mol/L. Excitation wavelengths correspond to absorption maximum $\lambda_{max}$. [c] Fluorescence quantum yields measured using a 0.1 M $H_2SO_4$ solution of quinine sulphate ($\Phi_F$ = 0.54) as a reference.[13]

Both the extreme strengthening of the bridge NH-X=C- linker conjugation in **ETZ 1d** and the replacement of the NH hydrogen atom with methyl groups in **ETZ 1j** decrease the emission intensity (Table 5, entries 4 and 10). Incorporating the fluorescent carbazole moiety into the structure of **TZ 1h** results in a bathochromic shift in the absorption spectrum up to 390 nm (Table 5, entry 8) but substantially decreases the Stokes shift.

## Theoretical calculations of the absorption and emission

To gain further insight into the effect of different substituents and the structure of the bridged linear chain (enamine/aza-enamine) linking the thiazole ring and aromatic cycle **A** on the conformational properties in compounds **1** and **2**, we performed an extensive quantum mechanical investigation considering the geometry of the ground and excited states. The optimized geometries of the *Z*,*Z*-isomers of thiazoles **1a-g**,**i** and **2a**,**c**,**d** in dioxane are shown in Figure S28. Selected bond lengths, bond angles and torsion angles of **1a-g**,**i** and **2a**,**c**,**d** are provided in Tables S6 and S7 (SI).

The optimized geometries show the planarity between the enamine/aza-enamine chain and the cyano group and thiazole fragment (see Table S5, Figure S29) and the twisting of aromatic cycle **B** in the ground state ($\theta_2$ = 22.4 – 42.1°). The geometry of cycle **A** is different in the structures of **ETZ**s **1a-g**,**i** and **ATZ**s **2a**,**c**,**d**. Whereas the geometries of the **ETZ**s exhibit substantial torsion angles ($\theta_1$ = 17.7-51.6°), the geometries of the **ATZ**s show very small torsion angles (approximately $\theta_1$ =2.61-2.62°). We can conclude that this aromatic ring participates in the whole conjugated systems of compounds **2a**,**c**,**d** and is the reason for the bathochromic shift in the absorption band compared to the **ETZ**s (Table 5). The largest deviation from planarity for the aromatic ring **A** is observed in compounds bearing one or two substituents in the ortho-positions (49.0 – 51.6°), i.e., **1f** and **1e**, which had the most blueshifted absorption bands. **ETZ 1d** is one exception from this general trend. The structure of this compound is more planar due to strong conjugation (8.9° in dioxane and 6.8° in ethanol).

Extensive changes occurred during excitation, particularly the torsion angle $\theta_1$ in **ETZ**s **1a-c,e-g**,**i** geometry, which considerably decreased (to 0.2°). However, one interesting exception was observed. The same ($\theta_1$) dihedral angle of **ETZ 1d** in ethanol (*GS*) was 6.8° in the ground state and 91.2° in the excited state (*ES*), a remarkable increase (Tables S6,S7 and Figure S28). This rotation has caused a considerable twisting of the 4-nitrophenyl aromatic ring ($R^1$ = 4-$NO_2C_6H_4$) during excitation and loss of emission intensity in this solvent.

The introduction of a second aromatic cycle (**C**) to the thiazole ring ($R^4$ = Ph) causes the formation of propeller-like structures for compounds **1i** and **2d** in the *GS* and *ES*, although more twisting was observed for **ETZ 1i** than for **ATZ 2d**. However, both compounds demonstrate decreasing lengths of the bonds linking aromatic cycles **A**, **B**, and **C** with the framework of the molecules because of the enhancing of the conjugated system and the redshifting the wavelengths in the absorption and emission spectra.

Notably, detailed analysis of the geometries of **ETZ**s **1** and **ATZ**s **2** shows the probability of the formation of different weak intramolecular interactions. The number of these interactions may vary depending on the structures of compounds **1** and **2**. The most substantial interaction involves the hydrogen in the central part of the molecule, as previously discussed and shown in Figures 3 and 7, both in the *GS* and *ES*.

The length of the N1H···$N_{TZ}$ hydrogen bond is shortened in the *GS* of compounds **1a-g**,**i** (1.949-1.981 Å) but is much shorter for **2a**,**c**,**d** (1.914-1.924 Å). Notably, for most of the thiazoles the hydrogen bond is strengthened in the *ES* (1.784-1.936 Å). Two exceptions are compounds **1d** (both in dioxane and in EtOH) and **1f**, where this bond length substantially increases from 1.949-1.975 Å in the *GS* to 2.002-2.084 Å in the *ES*.

.

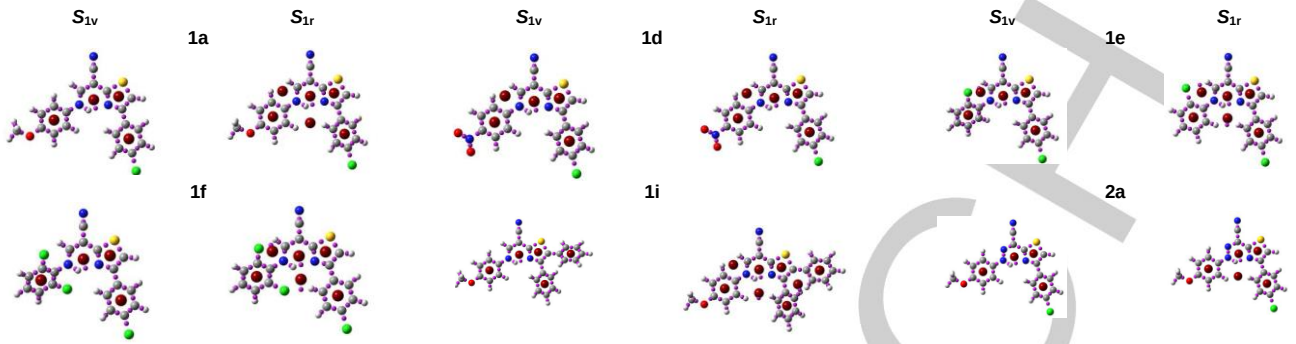


**Figure 7.** The critical points *ESs* ($S_{1v}$, $S_{1r}$) for **ETZs 1e**,**f**,**i** and **ATZ 2a** in dioxane. Colour legend for the atoms: white (H), grey (C), blue (N), red (O), and yellow (S); colour legend for CP: dark-red (RCP), pink (BCP).

The formation of the hydrogen bond is confirmed by applying the AIM theory[11] to analyse the intramolecular interactions in the structures of **ETZs 1** and **ATZs 2** in the *GS* and *ESs* (Figures 3 and 7 and additional examples in the SI, Figure S26). The BCP (bond critical point) (3, -1)-type for the N1H···N2 hydrogen bond and RCP (3, +1) for the pseudo-cycle, which was formed from the N2-C2-C1-X-N1-H chain of atoms in the *GS*, Franck-Condon *ES* ($S_{1v}$) and relaxed *ES* ($S_{1r}$), were found (Figure 7 and SI, S26). The AIM approach also confirms the formation of a C9H·· HC6 bond and a new additional ring: a pseudo-macrocycle constructed from the HC9-C7-N1-X-C1-C2-N2-C4-C5-C6H atom sequence, particularly for the relaxed *ES* ($S_{1r}$) of **ETZ**s **1a-c**,**d-h** and **ATZ**s **2a**,**c**.

Further analysis of the intramolecular interactions, which was performed according to the RDG index (SI, S27 and S29), supported most of the AIM theory predictions, including the additional strong hydrogen bond formation between the Cl atom at the ortho-position of the aromatic ring and C-proton of the enamine group in compound **1e**, which is an additional reason for the restricted rotation in this molecule.

The combined effects of the intramolecular interactions lead to strengthening of the rigidity in the **TZ**s in the *ES*, which can be evaluated by the decrease in their bond length. For instance, most of the σ-bonds in the structure of **TZ**s **1** and **2** have decreased their lengths during the $S_0 \rightarrow S_1$ transition to, on average, 94% of the original value. This conjugation is particularly reflected in the variations in the length of C-NH bond linking the aromatic ring **A** and the enamine chain. This bond length in **ETZ**s **1a-c,e-g,i** is shorter in the *ES* than in *GS*. However, the opposite trend is observed for the **ATZ**s; i.e., this bond length increases during excitation. These findings are very important for absorption and emission and help explain the differences in the optic characteristics of the **ETZ**s and **ATZ**s. Thus, we can conclude that photon absorption causes strengthening of the ICT character for **ETZ**s. Whereas **ATZ**s, on the contrary, demonstrated weakening ICT upon excitation.

The theoretically optimized energy and absorption and emission maxima, along with the oscillator strength, ground/excited state dipole moment modulus and angles formed by the dipole moment vectors, are provided in Table 6 and Table S8 (SI). The simulated absorption and emission maxima for all of the investigated compounds are consistent with the experimental values (Figures 5, 6, S24, S25, S30 and S31). The $S_0 \rightarrow S_1$ transitions, which are responsible for the largest absorption band, are mainly ascribed to the electronic transitions from the HOMO to LUMO for the derivatives, as confirmed by the orbital coefficients (*c*). One exception of this trend is **ETZ 1g** both in dioxane and in DMSO (Table 6, entry 9-12). The main electronic transition from the HOMO to the LUMO for this compound with the push-pull structure is accompanied by an additional transition from the HOMO to the LUMO + 1 (Table 6, Figure S32).

The calculated data show that (1) the $S_0 \rightarrow S_{1v}$ electron transition occurs more easily for compounds **1a**, **2d** and particularly **2a** with the push-pull conjugated system and highest oscillator strength; and (2) large changes occur in electronic distribution during excitation.

This difference emerges in the value of the dipole moments of the investigated compounds, which remarkably increases in the *ES*, particularly for enamines **1a**,**d**,**g**. Moreover, for **ETZ**s **1e**,**f**, and **ATZ**s **2a**,**d** it was accompanied by a substantial change in the angle of the dipole moment vector (Table 6). The substantial change in electronic distribution after the $S_0 \rightarrow S_{1v}$ excitation supports the plots showing the difference in electronic density between the *GS* and the first electronic *ES* of **1a-g**,**i** and **2a**,**c**,**d** in dioxane (SI, Figure S33).

To investigate the reactive sites of the **ETZ**s and **ATZ**s, their molecular electrostatic potential (MEP) was evaluated. The MEP surfaces in Figure 8 for several examples (additional examples are presented in the SI, Figure S34) show the sites of electrophilic and nucleophilic attack and hydrogen bonding interactions and the size, shape, and electrostatic potential distribution of the molecules. The MEP surface is a useful tool for investigating the *GS* and *ES*, especially regarding the effect of intermolecular interactions on absorption and emission. Consequently, the most active sites in the title compounds are used to rationalize their interactions with solvents or bioanalytes. Figures 8 and S34 (SI) show that in the *GS*, the CN and $NO_2$ groups gather negative charge, indicating that they are potential sites for electrophilic attack. Positive charge covers the MeO group in most compounds, except thiazole **1d**, where the positive charge is concentrated around the enamine NH group, and **ATZ 2c**, where the positive charge is localized on the thiazole and $R^3$-aromatic ring. Thus, these parts of the compounds are potential sites for nucleophilic attack.

A large difference is observed between the molecular surfaces in the *GS* and *ES*. Compounds **1d**,**g** and **2a**,**c**,**d** exhibit strong enlargement of and increase in the negative and positive active site areas, particularly **TZ**s **1d**,**g**, and **2a**,**d**. These observations enable us to select compounds **1a, 1d** and **1g** as representative examples to investigate (fluoro-)solvatochromic behaviour.

**Table 6.** Calculated absorption and emission properties[a] for (*Z*,*Z*)-**ETS**s **1a-g**,**i** and **ATS**s **2a**,**c**,**d** in dioxane.

| Entry | Comp | *n* | *c* | $\lambda_{0n}$ [nm] | $f_{0n}$ | $\mu_0$ [D] | $\mu_{nv}$ [D] | $\theta_{0,nv}$ [°] | *c'* | $\lambda_{10}$ [nm] | $f_{10}$ | $\mu_{1r}$ [D] | $\theta_{0,1r}$ [°] |
|---|---|---|---|---|---|---|---|---|---|---|---|---|---|
| 1 | **1a** | 1 | 0.69655 | 374.9 | 0.8338 | 4.2 | 7.8 | 9.9 | -0.70254 | 458.6 | 0.5650 | 9.1 | 16.1 |
| 2 | **1a**[b] | 1 | 0.69882 | 380.0 | 0.8702 | 7.3 | 13.1 | 42.6 | 0.70220 | 469.2 | 0.0417 | 18.2 | 60.7 |
| 3 | **1b** | 1 | 0.69593 | 367.8 | 0.5919 | 3.6 | 4.5 | 13.5 | 0.69740 | 422.1 | 0.5424 | 4.8 | 26.1 |
| 4 | **1c** | 1 | 0.69685 | 369.8 | 0.6579 | 2.3 | 3.8 | 5.4 | -0.69848 | 414.5 | 0.6100 | 4.3 | 11.3 |
| 5 | **1d** | 1 | 0.70399 | 398.7 | 0.4710 | 4.7 | 19.1 | 6.8 | 0.70443 | 503.7 | 0.3502 | 20.7 | 5.9 |
| 6 | **1d**[c] | 1 | 0.70511 | 396.9 | 0.4805 | 6.0 | 26.5 | 2.1 | 0.70477 | 838.7- | 0.0000 | 35.8 | 8.2 |
| 7 | **1e** | 1 | 0.68870 | 364.3 | 0.5093 | 4.9 | 5.4 | 35.4 | -0.69587 | 405.4 | 0.4901 | 6.2 | 36.3 |
| 8 | **1f** | 1 | 0.68682 | 350.1 | 0.4313 | 4.6 | 5.6 | 67.5 | 0.69274 | 406.3 | 0.3785 | 6.9 | 77.3 |
| 9 | **1g** | 1 | 0.70519 | 488.8 | 0.0496 | 4.5 | 26.9 | 26.9 | 0.70668[c] | 458.7 | 0.4111 | 27.1 | 26.3 |
| 10 | **1g** | 2 | 0.63073 | 375.2 | 0.5422 | 4.5 | 11.1 | 3.7 | - | - | - | - | - |
| 11 | **1g**[b] | 1 | 0.70633 | 567.0 | 0.0734 | 5.3 | 30.3 | 15.3 | 0.70978 | 453.4 | 0.0591 | 33.8 | 21.7 |
| 12 | **1g**[b] | 2 | 0.63884 | 377.6 | 0.2724 | | 26.8 | 17.6 | - | - | - | - | - |
| 13 | **1i** | 1 | 0.69572 | 384.2 | 0.5769 | 5.6 | 8.3 | 17.4 | 0.70362 | 458.7 | 0.8396 | 9.1 | 30.5 |
| 14 | **2a** | 1 | 0.70278 | 415.4 | 0.9144 | 3.3 | 8.8 | 39.5 | 0.70577 | 463.2 | 0.2598 | 7.9 | 37.6 |
| 15 | **2c** | 1 | 0.68992 | 409.9 | 0.6700 | 7.5 | 14.7 | 3.2 | 0.69501 | 480.6 | 0.4678 | 18.3 | 6.6 |
| 16 | **2d** | 1 | 0.70399 | 423.8 | 0.8026 | 5.4 | 9.3 | 48.1 | -0.70724 | 514.1 | 0.6820 | 9.0 | 51.2 |

[a] Computed orbital's coefficient (*c* and *c'*), absorption wavelength ($\lambda_{0n}$, nm), fluorescence wavelength ($\lambda_{10}$, nm), oscillator strength ($f_{0n}$ and $f_{10}$), modulus of the electric dipole moments of the ground state ($\mu_0$, D) and of the vertical FC excited state ($\mu_{nv}$, D), angles formed by the dipole moment vectors ($\theta_{0,nv}$ and $\theta_{0,1r}$ (°)). [b] in DMSO (IEF-PCM). [c] in MeCN (IEF-PCM).

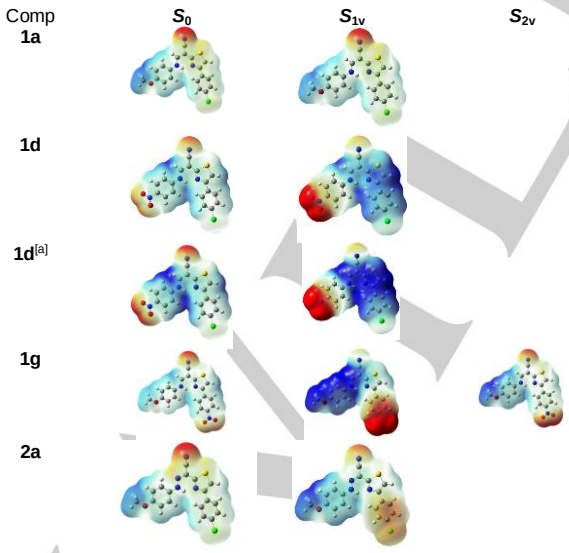


**Figure 8.** MEP plots of **ETZ**s **1a**,**d**,**g** and **ATZ**s **2a** in dioxane ([a] - in ethanol) in the *GS* and *ESs*. Negatively charged surfaces highlighted red and yellow colour and positively charged surfaces highlighted blue colour.

## (Fluoro-)Solvatochromism

The photophysical data for **ETZ**s **1a,1d** and **1g** in various solvents are shown in Table 7. The absorption and emission spectra of thiazoles **1a**, **1d** and **1g** are presented in Figure 9. The absorbance spectra in most solvents did not depend on the solvent properties, as shown in Table 7 and Figure 9, except compound **1d** in DMF. In this solvent, thiazole **1d** exhibits two long wavelength bands at 404 and 527 nm because of its stronger interaction with the polar solvent (Table 7, entry 16; Figure 9c).

By contrast, the fluorescence did strong depend on the nature of the solvents. The fluorescence band shows an upward shift of 39-89 nm for **1a,** and 69-139 nm for **1g** and 41-85 for **1g** with increasing solvent polarity. The greater stabilization of the excited singlet state occures in polar solvents and confirming their high polarity and ICT character in that state, in accordance with the calculation results (Table 7 and Table S8).

The quantum yields also respond to the variation in solvent properties. The emission intensity of thiazole **1a**, which shows a moderate change in its dipole moment modulus during excitation is highest in nonpolar, aprotic dioxane (Table 7, entry 2), but is completely quenched in dichloromethane (Table 7, entry 5).

**Table 7.** Photophysical characteristics of **ETZ**s **1a, 1d** and **1g** in selected solvents with different polarity.

| Entry | Comp | Solvent | $\lambda_{max}$ [a] [nm] | $\varepsilon_{max}$ [$M^{-1}$ $cm^{-1}$] | $\lambda_{em}$ [b][nm] | Stokes shift [nm/$cm^{-1}$] | $\Phi_F$ [%][c] |
|---|---|---|---|---|---|---|---|
| 1 | **1a** | Toluene | 377 | 26256 | 433 | 56/3431 | 0.26 |
| 2 | | Dioxane | 374 | 25342 | 458 | 84/4904 | 1.15 |
| 3 | | AcOEt | 373 | 28612 | 412 | 39/2538 | 0.40 |
| 4 | | THF | 374 | 22749 | 424 | 50/3153 | 0.18 |
| 5 | | $CH_2Cl_2$ | 375 | 24452 | - [d] | - | - |
| 6 | | DMSO | 379 | 44354 | 468 | 89/5018 | 0.15 |
| 7 | | DMF | 377 | 31280 | 430 | 53/3269 | 0.36 |
| 8 | | Acetone | 374 | 28169 | 414 | 40/2583 | 0.14 |
| 9 | | MeCN | 372 | 31146 | 423 | 51/3241 | 0.09 |
| 10 | | EtOH | 372 | 27986 | 412 | 40/2610 | 0.34 |
| 11 | **1d** | Toluene | 397 | 36077 | 466 | 69/ 112/5543 | 0.88 |
| 12 | | Dioxane | 397 | 33425 | 509 | 112/ 3730 | 0.43 |
| 13 | | AcOEt | 395 | 54628 | 501 | 106/5356 | 0.18 |
| 14 | | THF | 397 | 42460 | 498 | 101/5109 | 0.24 |
| 15 | | $CH_2Cl_2$ | 397 | 40110 | 536 | 139/6532 | 0.18 |
| 16 | | DMF | 404, 527 | 15574, 6318 | - [d] | - | - |
| 17 | | Acetone | 397 | 27536 | - [d] | - | - |
| 18 | | MeCN | 397 | 34380 | - [d] | - | - |
| 19 | | EtOH | 393 | 4966 | - [d] | - | - |
| 20 | **1g** | Toluene | 376 | 34465 | 439 | 63/3816 | 1.61 |
| 21 | | Dioxane | 374 | 28823 | 459 | 85/4952 | 2.05 |
| 22 | | AcOEt | 372 | 40635 | 426 | 54/3408 | 0.24 |
| 23 | | THF | 376 | 26775 | 417 | 41/2615 | 1.43 |
| 24 | | $CHCl_3$ | 372 | 27169 | -[d] | - | - |
| 25 | | DMF | 375 | 47020 | 439 | 64/3888 | 1.09 |
| 26 | | DMSO | 378 | 27102 | 452 | 74/4331 | 0.55 |
| 27 | | Acetone | 373 | 24731 | -[d] | - | - |

[a] UV-vis absorption wavelengths at room temperature and a concentration of $c$ = 5×$10^{-5}$ mol/L. [b] Fluorescence wavelengths at room temperature at a concentration of $10^{-6}$ mol/L. Excitation wavelengths correspond to absorption maximum $\lambda_{max}$. [c] Fluorescence quantum yields measured using a 0.1 M $H_2SO_4$.

For the emission intensity of **ETZs 1d** and **1g** which have the highest dipole moment modulus in the *ES* (Table 6 and Table S8), the best quantum yield is in low-polarity toluene and dioxane, whereas in polar solvents, such as DMF, acetonitrile, and acetone, they are non-fluorescent. The low emission intensity of **TZ**s **1** in ethanol can be caused by specific and non-specific solvent-solute interactions, which is strongest for the thiazole **1d** and induced rotation of the aromatic ring **A** in the Frank-Codon excited state, as shown in Figure S28.

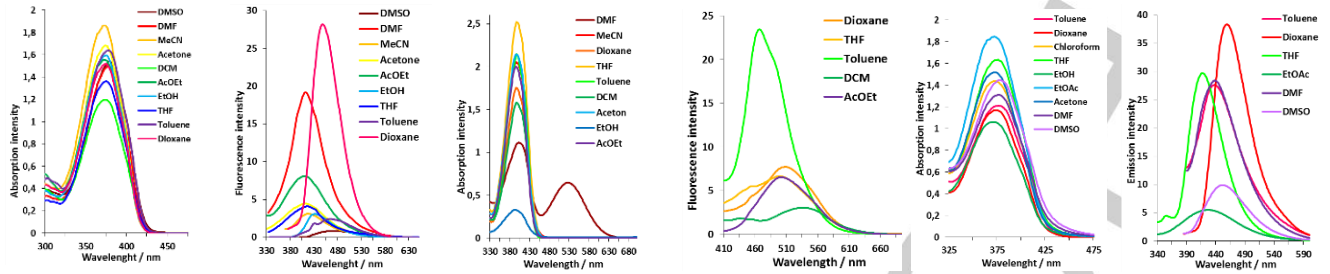


**Figure 9.** Absorption and emission spectra of thiazoles **1a** (a,b), **1d** (c,d) and **1g** (e,f) in different solvents at room temperature.

(Fluoro-)Solvatochromism is often interpreted in terms of simple analytical models, which consider the molecule as a point dipole placed at the centre of a spherical cavity.[7a] When the applicability conditions of these models are matched, it is possible to obtain regressions between the shift of the absorption (or emission) band (or the Stokes shift) and some function, expressing the solvent polarity, and from these regressions. If models are properly applied, useful information about the electric dipole moment of the molecule in the excited state may be extracted. Unfortunately our systems do not match the conditions requested for the applicability of those simple models, and any attempt to regress the fluorosolvatochromic data with any polarity function (*e.g.*, Lippert-Mataga, Bakhshiev, Kawsky-Chamma-Vallet, McRae, etc.) was unsuccessful. Simple continuum models do not offer a realistic surrounding and emission properties may be close to the experimental data and were able to accurately describe the ICT nature of representation, especially for complex systems or absorption and emission phenomena.[15] It was therefore necessary to make usage of the state-of-the-art quantum mechanical methods to obtain information about the nature of the excited state. The computational findings were extremely close to the experimental data (Tables 6,7 and Table S8) and were able to reveal and accurately describe the ICT nature of the transitions. It is evident, from spectral and calculation data, that compounds reported in this study exhibit strong dependence from the solvent polarity due to the ICT nature of the transition. Moreover, the strength of ICT character is easily tuned by varying type of electron withdrawing and electron donating substituents placed on the opposite moieties of the molecule. The strongest ICT is attributed to compounds **1d** and **1g**; this is confirmed by the experimental data.

Solvent viscosity may also affect the fluorescence of **TZ**s. This assumption is confirmed by the emission of **ETZ**s **1a**-**h** in the solid state (Figure 10). As shown in Figure 10, fluorescence at a maximum of approximately 479-490 nm was observed for powdered **ETZ**s **1a-h**. Because of intermolecular interactions in the solid state, the emission band of **ETZ**s **1** slightly shifts to longer wavelengths.

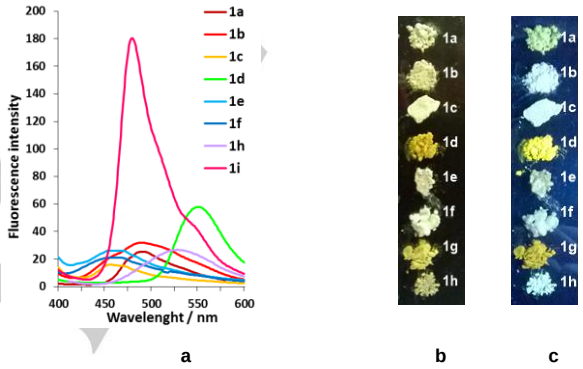


**Figure 10**. a - Emission spectra for **ETZs 1a-f**,**h**,**i** in the solid state at 25 °C. b - Photographs of powders of **ETZs 1a**-**g**,**i** in daylight and under irradiation. c - with a hand-held UV lamp at an emission wavelength of 380 nm.

## Conclusion

In summary, we synthesised new **TZ** derivatives (**ETZ**s and **ATZ**s) with conjugated -NH-CH=C< and -NH-N=C< linker that differ from each other by one atom and with the structure capable to form NH···$N_{Thiaz}$ intramolecular hydrogen bond. The synthesis of these compounds does not require severe conditions or expensive catalysts or reagents. Moreover, this method allowed us to obtain various compounds whose electronic structure may be controlled and tuned by varying the electronics and spatial parameters of the substituents. The fine structures and photophysical characteristics of **ETZ**s and **ATZ**s were investigated in detail using experimental (spectral) and theoretical (calculation) data. It should be emphasized that the theoretical and experimental data for the position and shape of the absorption and emission bands are consistent. Experimental and computational results based on analysis of the HOMO-LUMO distribution, the modulus of the dipole moment and its direction upon excitation of the investigated compounds highlight the presence of ICT state, which is especially polar for the excited state of compounds **1d** and **1g.** The formation of a series of weak intramolecular interactions in the *GS* and *ES* are confirmed by mean of the AIM theory and the NCI analysis.

The difference in the geometries of the **ETZ**s and **ATZ**s are essential and lead to differences in electronic contribution and, as a result, in their absorption and emission behaviour. For example, the fluorescence of the **ETZ**s is more intensive than that of the **ATZ**s. As a result, we can conclude that the small differences in

structure between the investigated compounds (i.e., replacing the carbon in the linear chain with a nitrogen atom and changing the nature or position of the substituents in the aromatic rings) lead to considerable changes in the photophysical properties of the investigated **TZs** ($\lambda_{abs}$, $\lambda_{em}$, quantum yield, Stokes shift, solid-state fluorescence, and environmental sensitivity) because of the variation in their conjugated systems and polarity, as well as the value, number and strength of their weak intramolecular interactions. The weakened hydrogen bonding in the *ES* (for the compounds **1d**, **2a-d**) or the impossibility of their formation (for compound **1h**) substantially decreases the emission intensity.

The computational results (polarity, MEP and HOMO-LUMO distribution) are encouraging about the perspective to create **ETZ**-based compounds whose absorption and emission properties may be extremely sensitive to their surrounding microenvironment. This feature was confirmed both by calculation (MEP) data and (fluoro-)solvatochromic investigations for the several examples. Moreover, the structures of the **ETZ**s and **ATZ**s include a convenient combination of functionalities and thus may be used both as useful building blocks in heterocyclic chemistry and as multidonor ligands for constructing different types of complexes, particularly valuable organometallic frameworks and functional materials.

Thus, we have demonstrated the accessibility of small thiazole derivatives with aryl enamine and aryl aza-enamine side groups and elucidated methods to design and synthesize new effective molecular fluorophore candidates for further application as analytes/bioanalytes because of their emission in solution and in the solid state.

## Experimental Section

**General**: All reactants were obtained from Acros Organics and used without further purification. $^1$H NMR and $^{13}$C NMR spectra were recorded with a Bruker Avance II (Karlsruhe, Germany) (400 MHz for $^1$H, 100 MHz for $^{13}$C) spectrometer. The chemical shifts are reported in parts per million (ppm) relative to TMS in $^1$H NMR and to the residual solvent signals in $^{13}$C NMR. The coupling constant (*J*) values are given in hertz (Hz). The signal splitting patterns are described as a singlet (s), doublet (d), triplet (t), quartet (q), sextet (sext), quintet (quin), multiplet (m), broad (br), doublet of doublets (dd), doublet of triplets (dt) or AA'XX' - spin system of *para*-substituted benzene with two different substituents. The major isomer signal is highlighted with an asterisk (*). The $^{13}$C NMR signal patterns for several compounds were by APT (attached proton test) and are described as follows: + for secondary or quaternary carbon atoms (positive signal) and - for primary or tertiary carbon atoms (negative signal). Mass spectra were recorded on a Shimadzu GCMS-QP 2010 “Ultra” (Kyoto, Japan) mass spectrometer using the electron impact (EI) ionization technique (40-200 °C, 70 eV). The abbreviation $[M]^+$ refers to the molecular ion. IR spectra were obtained on an FTIR-ATR (attenuated total reflection, ZnSe) spectrometer (neat) in the 4000-400 cm$^{-1}$ region (Ettlingen, Germany). Elemental analysis was conducted on a CHNS/O Perkin-Elmer 2400 Series II analyzer instrument (Shelton, CT USA). The melting points were determined on a Stuart SMP3 apparatus (Staffordshire, ST15 OSA, UK). The reactions were monitored by analytical thin-layer chromatography (TLC) on aluminium-backed silica-gel plates (Sorbfil UV–254). The components were visualized by short wavelength UV light (254 nm). The solvents were dried and distilled according to common procedures. All solvents were of spectroscopic grade.
The title products were purified by column chromatography on silica gel (0.035–0.070, 60 Å) and recrystallized from ethanol.

Thioacetamide (**3**), dimethylaminopropenethioamide (**4**) and arylhydrazonethioacetamides **8** were prepared using procedures reported in the literature.[6,9b,10] Full experimental details for synthesis of arylaminothioacrylamides **6a-h**, $^1$H NMR and $^{13}$C NMR spectra of new compounds (**6a-h, 1a-j** and **2a-d**), photophysical characterization, quantum mechanical calculation data are reported in the Supporting Information.

**General procedure for the synthesis of thiazoles 1a-j, 2a-d.** Halocarbonyl compound **7a-c** (0.26 g, 1.15 mmol) is added to the solution of thioamide **6a-h** or **8a-c** (0.25 g, 1.10 mmol) in DMF (2.0 ml). The mixture is kept at 80 °C for 0.5-4.0 h, then diluted with ethanol (12.5 ml) and kept at 10-12 °C for 30 min. The precipitate is collected by filtration.

**2-(4-(4-Chlorophenyl)thiazol-2-yl)-3-((4-methoxyphenyl)amino)-acrylonitrile (1a):** Bright yellow powder (0.263 g, 65%); mp 249-250 °C; IR (NPVO, ZnSe): $\tilde{\nu}$ = 3101 (NH), 3012, 2987, 2958, 2936, 2905, 2830 (CH), 2199 cm$^{-1}$ (CN); $^1$H NMR (400 MHz, DMSO-$d_6$, TMS): $\delta_H$ = 11.63* and 10.51 (both d, *J* = 13.1Hz, 1H, NHCH), 8.38* and 8.33 (both d, *J* = 13.1 Hz, 1H, CHNH), 8.00-7.98 (m, 2H, $H_{Ar}$), 8.05* and 7.91 (both s, 1H, CH), 7.55* and 7.50 (both d, *J* = 8.5 Hz, 2H, $H_{Ar}$), 7.39-7.34 (m, 2H, $H_{Ar}$), 7.01-6.95 (m, 2H, $H_{Ar}$), 3.77* and 3.76 ppm (both s, 3H, OMe); 9:1 mixture of isomers; $^{13}$C NMR (100 MHz, DMSO-$d_6$) $\delta_C$ = 164.9, 156.7, 152.9, 144.5, 133.0, 132.6, 128.9 (2C), 127.7 (2C), 119.5, 118.6 (2C), 115.2 (2C), 111.5, 76.6, 55.6 ppm; MS (EI) m/z (%): 367 ($M^+$, 100); elemental analysis calcd (%) for $C_{19}H_{14}ClN_3OS$: C 62.04, H 3.84, N 11.42; found: C 61.8, H 4.0, N 11.2.

**2-(4-(4-Chlorophenyl)thiazol-2-yl)-3-(phenylamino)acrylonitrile (1b):** Beige powder (0.312 g, 84%); mp 254-255 °C; IR (NPVO, ZnSe): $\tilde{\nu}$ = 3050, 3026, 2955, 2917 (CH), 2200 cm$^{-1}$ (CN); $^1$H NMR (400 MHz, DMSO-$d_6$, TMS): $\delta_H$ = 12.12 and 11.81* (both d, *J* = 12.9 Hz, 1H, NHCH), 9.31 and 8.44* (both d, *J* = 12.9 Hz, 1H, CHNH), 7.98-7.93 (m, 3H, $H_{Ar}$+CH), 7.60-7.50 (m, 2H, $H_{Ar}$), 7.46-7.37 (m, 4H, $H_{Ar}$), 7.16-7.12 ppm (m, 1H, $H_{Ar}$); 10:1 mixture of isomers; $^{13}$C NMR (100 MHz, DMSO-$d_6$) $\delta_C$ = 165.0 (+), 152.7 (+), 144.1 (-), 143.5 (+), 140.6 (+), 132.9 (+), 129.0 (2C) (-), 127.7 (2C) (-), 119.8 (+), 119.7 (-), 118.2 (2C) (-), 116.6 (2C) (-), 111.5 (-), 76.0 (+) ppm; MS (EI) m/z (%): 337 ($M^+$, 100); elemental analysis calcd (%) for $C_{19}H_{12}ClN_3S$: C 64.00, H 3.58, N 12.44; found: C 63.7, H 3.7, N 12.1.

**3-((4-Chlorophenyl)amino)-2-(4-(4-chlorophenyl)thiazol-2-yl)acrylo-nitrile (1c):** Beige powder (0.328 g, 80%); mp 256-257 °C; IR (NPVO, ZnSe): $\tilde{\nu}$ = 3112, 3059, 2999 (CH), 2199 cm$^{-1}$ (CN); $^1$H NMR (400 MHz, DMSO-$d_6$, TMS): $\delta_H$ = 11.78* and 10.47 (both d, *J* = 12.8Hz, 1H, NHCH), 8.47-8.39 (m, 1H, CHNH), 8.00-7.95 (m, 3H, $H_{Ar}$+CH), 7.51-7.49 (m, 2H, $H_{Ar}$), 7.44-7.35 ppm (m, 4H, $H_{Ar}$); 6:1 mixture of isomers; $^{13}$C NMR (100 MHz, DMSO-$d_6$) $\delta_C$ = 164.3, 152.9, 144.0, 138.0, 132.9, 132.1, 129.5 (2C), 129.0 (2C), 127.8 (2C), 118.7 (2C), 112.2, 78.0 ppm; MS (EI) m/z (%): 371 ($M^+$, 100); elemental analysis calcd (%) for $C_{18}H_{11}Cl_2N_3S$: C 58.08, H 2.98, N 11.29; found: C 57.8, H 3.1, N 11.1.

**2-(4-(4-Chlorophenyl)thiazol-2-yl)-3-((4-nitrophenyl)amino)-acrylo-nitrile (1d):** Yellow powder (0.312 g, 74%); mp 278-279 °C; IR (NPVO, ZnSe): $\tilde{\nu}$ = 3115 (NH), 3071, 3031, 3001, 2961 (CH), 2204 cm$^{-1}$ (CN); $^1$H NMR (400 MHz, DMSO-$d_6$, TMS): $\delta_H$ = 11.98* and 10.85 (both d, *J* =13.0 Hz, 1H, CHNH), 8.64* and 8.55 (both d, *J* = 13.0Hz, 1H, CHNH), 8.27* and 8.22 (both d, *J* = 8.5 Hz, 2H, $H_{Ar}$), 8.05-7.99 (m, 2H, $H_{Ar}$), 8.10* and 7.94 (both s, 1H, CH), 7.66-7.59 (m, 2H, $H_{Ar}$), 7.55* and 7.45 ppm (both d, *J* = 8.6 Hz, 2H, $H_{Ar}$); 1:4 mixture of isomers; $^{13}$C NMR (100 MHz, DMSO-$d_6$) $\delta_C$ = 164.1 (+), 153.8 (+), 143.6 (-), 145.2 (+), 143.3 (+), 133.6 (+), 132.5 (+), 129.6 (2C) (-), 128.4 (2C) (-), 126.2 (2C) (-), 119.2 (+), 117.5 (2C) (-), 113.8 (-), 81.1 (+) ppm; MS (EI) m/z (%): 382 ($M^+$, 100); elemental analysis calcd (%) for $C_{18}H_{11}ClN_4O_2S$: C 56.47, H 2.90, N 14.64; found: C 56.2, H 3.1, N 14.3.

**3-((2-Chlorophenyl)amino)-2-(4-(4-chlorophenyl)thiazol-2-yl)acrylo-nitrile (1e):** Pale yellow crystal (0.339 g, 83%); mp 231-232 °C; IR (NPVO, ZnSe): $\tilde{\nu}$ = 3164, 3113, 3076, 2921, 2852 (CH), 2204 cm$^{-1}$ (CN); $^1$H NMR (400 MHz, DMSO-$d_6$, TMS): $\delta_H$ = 11.86 (d, *J* = 12.6Hz, 1H, NH), 8.53 (d, *J* = 12.6Hz, 1H, CH), 8.04-8.07 (m, 3H, CH+$H_{Ar}$), 7.84 (d, *J* = 7.9 Hz, 1H, $H_{Ar}$), 7.54 (dd, *J* = 1.2, 8.0 Hz, 1H, $H_{Ar}$), 7.49 (d, *J* = 8.5 Hz, 2H, $H_{Ar}$), 7.42 (t, *J* = 7.4 Hz, 1H, $H_{Ar}$), 7.17 ppm (dt, *J* = 1.2, 8.0 Hz, 1H, $H_{Ar}$); $^{13}$C NMR (100 MHz, DMSO-$d_6$) $\delta_C$ = 164.2, 153.6, 143.2, 136.2, 133.2, 132.3, 129.8, 128.6 (2C), 128.0 (2C), 125.1, 121.4, 118.9, 117.0, 112.8, 79.8 ppm; MS (EI) m/z (%): 371 ($M^+$, 100); elemental analysis calcd (%) for $C_{18}H_{11}Cl_2N_3S$: C 58.08, H 2.98, N 11.29; found: C 57.8, H 3.2, N 11.0.

**2-(4-(4-Chlorophenyl)thiazol-2-yl)-3-((2,6-dichlorophenyl)amino)-acrylonitrile (1f):** Pale yellow powder (0.357 g, 80%); mp 256-257 °C; IR (NPVO, ZnSe): $\tilde{\nu}$ =3106 (CH), 2214 cm$^{-1}$ (CN); $^1$H NMR (400 MHz, DMSO-

$d_6$, TMS): $\delta_H$ = 11.36 (d, *J* = 12.4 Hz, 1H, NH), 8.13-8.11 (m, 2H, 2CH), 8.05 (d, *J* = 8.5 Hz, 1H, $H_{Ar}$), 7.63 (d, *J* = 8.2 Hz, 1H, $H_{Ar}$), 7.50 (d, *J* = 8.6 Hz, 2H, $H_{Ar}$), 7.36 ppm (t, *J* = 8.2 Hz, 1H, $H_{Ar}$); $^{13}$C NMR (100 MHz, DMSO-$d_6$) $\delta_C$ = 164.7, 153.9, 149.6, 135.0, 133.6, 132.6, 129.9 (2C), 129.3 (2C), 129.2 (2C), 128.6, 128.4 (2C), 119.2, 112.9, 78.5 ppm; MS (EI) m/z (%): 404 ($M^+$, 100); elemental analysis calcd (%) for $C_{18}H_{10}Cl_3N_3S$: C 53.16, H 2.48, N 10.33; found: C 52.9, H 2.6, N 10.1.

**3-((4-Methoxyphenyl)amino)-2-(4-(4-nitrophenyl)thiazol-2-yl)-acrylonitrile (1g):** Orange powder (0.279 g, 67%); mp 276-277 °C; IR (NPVO, ZnSe): $\tilde{\nu}$ = 3106 (NH), 2988, 2940, 2913, 2831 (CH), 2200 cm$^{-1}$ (CN); $^1$H NMR (400 MHz, DMSO-$d_6$, TMS): $\delta_H$ = 11.63* and 10.43 (both d, *J* = 13.1 Hz, 1H, NHCH), 8.82* and 8.12 (both s, 1H, CH), 8.41-8.35 (m, 3H, $H_{Ar}$+CH), 8.25-8.22 (m, 2H, $H_{Ar}$), 7.40* и 7.32 (both d, *J* = 8.9 Hz, 2H, $H_{Ar}$), 6.97* and 6.93 (both d, *J* = 8.9 Hz, 2H, $H_{Ar}$), 3.80* and 3.79 ppm (both s, 3H, OMe); 9:1 mixture of isomers; $^{13}$C NMR (100 MHz, DMSO-$d_6$) $\delta_C$ = 165.5 (+), 156.8 (+), 151.9 (+), 147.1 (+), 144.8 (-), 139.3 (+), 132.5 (+), 127.1 (2C) (-), 124.2 (2C) (-), 119.5 (+), 118.7 (2C) (-), 115.2 (2C) (-), 114.9 (-), 76.3 (+), 55.5 (-) ppm; MS (EI) m/z (%): 378 ($M^+$, 100); elemental analysis calcd (%) for $C_{19}H_{14}N_4O_3S$: C 60.31, H 3.73, N 14.81; found: C 60.1, H 3.9, N 14.5.

**2-(4-(4-Chlorophenyl)thiazol-2-yl)-3-((9-ethyl-9*H*-carbazol-3-yl)-amino)acrylonitrile (1h):** Brown powder (0.340 g, 68%); mp 290-291 °C; $^1$H NMR (400 MHz, DMSO-$d_6$, TMS): $\delta_H$ = 11.97 (d, *J* = 13.1 Hz, 1H, NHCH), 8.50 (d, *J* = 13.0 Hz, 1H, NHCH), 8.25 (d, *J* = 2.1 Hz, 1H, $H_{Ar}$), 8.14 (dd, *J* = 2.1, 7.7 Hz, 1H, $H_{Ar}$), 8.02 (d, *J* = 8.6 Hz, 1H, $H_{Ar}$), 7.89 (s, 1H, CH), 7.57-7.42 (m, 6H, $H_{Ar}$), 7.20 (t, *J* = 7.1Hz, 1H, $H_{Ar}$), 4.45 (q, *J* = 7.1Hz, 2H, $CH_2$), 1.42 ppm (t, *J* = 7.1Hz, 3H, Me); $^{13}$C NMR (100 MHz, DMSO-$d_6$) $\delta_C$ = 165.0, 152.8, 144.7, 140.3, 137.1, 132.9, 132.3, 131.5, 129.0 (2C), 127.8 (2C), 126.2, 123.0, 121.9, 120.7, 119.9, 118.8, 116.7, 111.4, 110.1, 109.3, 108.4, 76.1, 37.1, 13.6 ppm; MS (EI) m/z (%): 454 ($M^+$, 100); elemental analysis calcd (%) for $C_{26}H_{19}ClN_4S$: C 68.64, H 4.21, N 12.31; found: C 68.7, H 4.1, N 12.0.

**2-(4,5-Diphenylthiazol-2-yl)-3-((4-methoxyphenyl)amino)acrylonitrile (1i):** Yellow powder (0.450 g, 70%); mp 270-271 °C; IR (NPVO, ZnSe): $\tilde{\nu}$ = 3058, 3029, 2952, 2937, 2902, 2805 (CH), 2201 cm$^{-1}$ (CN); $^1$H NMR (400 MHz, DMSO-$d_6$, TMS): $\delta_H$ = 11.90 (d, *J* = 12.9Hz, 1H, NHCH), 8.34 (d, *J* =13.0Hz, 1H, NHCH), 7.53-7.51 (m, 2H, $H_{Ar}$), 7.38-7.34 (m, 8H, $H_{Ar}$), 7.23 and 6.93 (AA'XX', *J* = 8.9Hz, 4H, $H_{Ar}$), 3.78 ppm (s, 3H, OMe). $^{13}$C NMR (100 MHz, DMSO-$d_6$) $\delta_C$ = 163.0, 157.1, 149.2, 145.2, 134.5, 132.4, 131.3, 129.9 (2C), 129.5 (2C), 129.3, 129.1, 129.0 (2C), 128.9 (2C), 128.7, 120.0, 118.8 (2C), 115.7 (2C), 76.4, 56.0 ppm; MS (EI) m/z (%): 409 ($M^+$, 100); elemental analysis calcd (%) for $C_{25}H_{19}N_3OS$: C 73.33, H 4.68, N 10.26; found: C 73.1, H 4.8, N 10.0.

**2-(4-(4-Chlorophenyl)thiazol-2-yl)-3-(methyl(phenyl)amino)acrylo-nitrile (1j):** Beige powder (0.271 g, 70%); mp 165-167 °C; $^1$H NMR (400 MHz, DMSO-$d_6$, TMS): $\delta_H$ = 8.24 (s, 1H, CH), 7.92 (d, *J* = 8.6 Hz, 2H, $H_{Ar}$), 7.73 (s, 1H, CH), 7.50-7.46 (m, 2H, $H_{Ar}$), 7.39 (t, *J* = 7.3 Hz, 4H, $H_{Ar}$), 7.32 (t, *J* = 7.3 Hz, 1H, $H_{Ar}$), 3.82 ppm (s, 3H, Me); $^{13}$C NMR (100 MHz, DMSO-$d_6$) $\delta_C$ = 166.1, 153.2, 149.1, 145.8, 133.3, 133.0, 130.1 (3C), 129.2 (2C), 128.2 (2C),127.4, 123.5, 118.5, 112.0, 76.5, 41.6 ppm; MS (EI) m/z (%): 351 ($M^+$, 100); elemental analysis calcd (%) for $C_{19}H_{14}ClN_3S$: C 64.86, H 4.01, N 11.94; found: C 64.6, H 4.3, N 11.6.

**4-(4-Chlorophenyl)-*N*-(4-methoxyphenyl)thiazole-2-carbohydrazo-noyl cyanide (2a):** Bright orange powder (0.260 g, 64%); mp 177-178 °C; $^1$H NMR (400 MHz, DMSO-$d_6$, TMS): $\delta_H$ = 13.93 and 11.84* (both s, 1H, NH), 8.37* and 8.06 (both s, 1H, CH), 8.04-7.98 (m, 2H, $H_{Ar}$), 7.55 and 7.47* (both d, *J* = 8.3 Hz, 2H, $H_{Ar}$), 7.40-7.38 (m, 2H, $H_{Ar}$), 6.99 and 6.94 (both d, *J* = 8.8 Hz, 2H, $H_{Ar}$), 3.80 and 3.77* ppm (both s, 3H, Me); 3:2 mixture of isomers; $^{13}$C NMR (100 MHz, DMSO-$d_6$) $\delta_C$ = 163.7*/159.6, 156.8/156.1*, 153.9/153.2*, 136.0*/134.9, 133.5/132.8*, 132.5*/131.0, 129.1/128.8* (2C), 128.0/127.7* (2C), 116.9*/116.8 (2C), 115.0/114.8 (2C), 114.7*, 110.7*, 107.1*/105.6, 55.4* ppm; mixture of isomers. MS (EI) m/z (%): 368 ($M^+$, 58); elemental analysis calcd (%) for $C_{18}H_{13}ClN_3OS$: C 58.62, H 3.55, N 15.19; found: C 58.4, H 3.7, N 14.9.

**4-(4-Chlorophenyl)-*N*-phenylthiazole-2-carbohydrazonoyl cyanide (2b):** Bright yellow powder (0.320 g, 86%); mp 184-185 °C; $^1$H NMR (400 MHz, DMSO-$d_6$, TMS): $\delta_H$ = 13.98* and 11.85 (both s, 1H, NH), 8.39* (s, 1H, CH), 8.05-7.99 (m, 2H, $H_{Ar}$), 7.55* and 7.16 (both d, *J* = 8.6Hz, 2H, $H_{Ar}$), 7.46-7.41 (m, 4H, $H_{Ar}$), 7.34* and 7.06 ppm (both t, *J* = 8.4 Hz, 1H, $H_{Ar}$); 2:1 mixture of isomers; $^{13}$C NMR (100 MHz, DMSO-$d_6$) $\delta_C$ = 163.4*/159.3, 153.9/153.2*, 142.3*/141.2, 133.5/132.8*, 132.4*/131.3, 129.6/129.4* (2C), 129.1/128.8* (2C), 128.0/127.6* (2C), 124.7/123.6*, 116.5*/116.4, 115.3*/115.1 (2C), 108.4*/106.8, 110.5* ppm; mixture of isomers; MS (EI) m/z (%): 338 ($M^+$, 49); elemental analysis calcd (%) for $C_{17}H_{11}ClN_4S$: C 60.27, H 3.27, N 16.54; found: C 60.0, H 3.4, N 16.3.

**4-(4-Chlorophenyl)-*N*-(4-nitrophenyl)thiazole-2-carbohydrazonoyl cyanide (2c):** Bright yellow powder (0.359 g, 85%); mp 288-290 °C; $^1$H NMR (400 MHz, DMSO-$d_6$, TMS): $\delta_H$ = 14.00 and 12.33* (both s, 1H, NH), 8.28 and 8.23* (both d, *J* = 9.2 Hz, 2H, $H_{Ar}$), 8.17* and 7.93 (both s, 1H, CH), 8.08 and 8.01* (both d, *J* = 8.6 Hz, 2H, $H_{Ar}$), 7.64 and 7.60* (both d, *J* = 9.2 Hz, 2H, $H_{Ar}$), 7.55 and 7.46* ppm (both d, *J* = 8.6 Hz, 2H, $H_{Ar}$); 3:1 mixture of isomers; $^{13}$C NMR (100 MHz, DMSO-$d_6$) $\delta_C$ = 162.4, 153.7, 147.8, 142.4, 133.0, 132.2, 128.9 (2C), 127.7, 125.6 (2C), 116.4(2C), 115.0 (2C), 112.6, 109.9 ppm; MS (EI) m/z (%): 383 ($M^+$, 64); elemental analysis calcd (%) for $C_{17}H_{10}ClN_5O_2S$: C 53.20, H 2.63, N 18.25; found: C 52.9, H 2.8, N 17.9.

***N*-(4-methoxyphenyl)-4,5-diphenylthiazole-2-carbohydrazonoyl cyanide (2d):** Brown powder (0.338 g, 75%); mp 167-169 °C; $^1$H NMR (400 MHz, DMSO-$d_6$, TMS): $\delta_H$ = 11.11 and 11.79* (both s, 1H, NH), 7.56-7.50 (m, 2H, $H_{Ar}$), 7.41-7.28 (m, 10H, $H_{Ar}$), 6.97 and 6.89* (both d, *J* = 9.0Hz, 2H, $H_{Ar}$), 3.80 and 3.78 ppm (both s, 3H, Me); 2:1 mixture of isomers; $^{13}$C NMR (100 MHz, DMSO-$d_6$) $\delta_C$ = 161.3*/157.2 (+), 156.7/156.0* (+), 149.7/149.4* (+), 136.0*/134.8 (+), 134.1*/133.0, 132.9/132.0* (+), 130.9*/129.8, 129.5/129.2* (2C) (-), 129.0* (2C) (-), 128.7*/128.6 (2C) (-), 128.6*/128.5 (2C) (-), 128.4*/128.1 (2C) (-), 116.8/110.7* (+), 116.5* (2C) (-), 115.0*/114.7 (2C) (-), 106.8*/105.5 (+), 55.3/55.2* (-) ppm; mixture of isomers; MS (EI) m/z (%): 410 ($M^+$, 71); elemental analysis calcd (%) for $C_{24}H_{18}N_4OS$: C 70.22, H 4.42, N 13.65; found: C 69.9, H 4.6, N 13.4.

### Electronic absorption and emission spectroscopy

UV-vis absorption spectra were recorded on a Perkin-Elmer Lambda 35 UV-vis spectrophotometer (Shelton, CT, USA). The fluorescence of the sample solutions was measured on a Hitachi F-7000 spectrophotometer (Tokyo, Japan). The absorption and emission spectra were recorded in 1,4-dioxane, toluene, acetone, MeCN, THF, DCM, DMF, DMSO, EtOH and AcOEt using 10.00 mm quartz cells. The excitation wavelength was the absorption maxima. The atmospheric oxygen contained in solutions was not removed. The concentrations of the compounds in solution were $5\times10^{-5}$ M and $10^{-6}$ M for absorption and fluorescence measurements, respectively. The relative fluorescence quantum yields ($\Phi_F$) were determined using quinine sulfate ($10^{-5}$ M) in 0.1 M $H_2SO_4$ as a standard ($\Phi_F$ = 0.546).[13]

## Acknowledgements

The research was supported by the Government of the Russian Federation (Act 211, contract # 02.A03.21.0006). K. L. Thanks RFBR for funding № 16-33-00327 mol_a. E. B. thanks the Italian "Ministero per l'Università e la Ricerca Scientifica e Tecnologica" for fundings [FIRB 2013, RBFR13PSB6].

**Keywords:** Thiazoles; Fluorescence; Solvatochromism; Hydrogen bond; Density functional theory

## References:

[1] a) M. T. Chhabria, Sh. Patel, P. Modi, P. S. Brahmkshatriya, *Curr. Top. Med. Chem.* **2016**; *26*, 2841-2862; b) C. B. Mishra, S. Kumari, M. Tiwari, *Eur. J. Med. Chem.* **2015**, *92*, 1-34; c) A. M. Matos, A. P. Francisco, *ChemMedChem* **2013**, *8*, 1751-1765.

[2] a) O. Seitz, F. Bergmann, D. A. Heindl, *Angew. Chem. Int. Ed.* **1999**, *38*, 2203-2206; b) O. Köhler, O. Seitz, *Chem. Commun.* **2003**, *23*, 2938-

2939; c) O. Köhler, D. V. Jarikote, O. Seitz, *ChemBioChem* **2005**, *6*, 69–77.

[3] a) F. Bellina, C. Manzini, G. Marianetti, C. Pezzetta, E. Fanizza, M. Lessi, P. Minei, V. Barone, A. Pucci, *Dyes and Pigm.* **2016**, *134*, 118-128; b) R. P. Tayade, N. Sekar, *J. Fluoresc.* **2016**, *26*, 1-14; c) R. Kammel, O. Tarabova, O. Machalický, M. Nepraš, B. Flumarová, J. Hanusek, *Dyes and Pigm*. **2016**, *128*, 101-110; d) K. Yamaguchi, T. Murai, S. Hasegawa, Y. Miwa, S. Kutsumizu, T. Maruyama,T. Sasamori, N. Tokitoh, *J. Org. Chem*. **2015**, *80*, 10742-10756; e) T. Tao, B.-B. Ma, Y.-X. Peng, X.-X. Wang, W. Huang, X.-Z. You, *J. Org. Chem.* **2013**, *78*, 8669–8679; f) S. Wolfram, H. Würfel, S. H. Habenicht, C. Lembke, P. Richter, E. Birckner, R. Beckert, G. Pohnert, *Beilstein J. Org. Chem*. **2014**, *10*, 2470-2479.

[4] a) P. Arora, R. Narang, S. K. Nayak, S. K. Singh, V. Judge, *Med. Chem. Res*. **2016**, *25*, 1717-1743; b) A. Ayati, S. Emami, A. Asadipour, A. Shafiee, A. Foroumadi, *Eur. J. Med. Chem.* **2015**, *97*, 699-718.

[5] N. K. Downer-Riley, Y. A. Jackson, *Curr. Top. Med. Chem*. **2016**, *16*, 3617-3626.

[6] I. V. Paramonov, N. P. Belskaia, V. A. Bakulev, *Chem. Het. Comp*. **2003**, *39*, 1385-1395.

[7] a) B. Valeur, M. N. Berberan-Santos, *Molecular Fluorescence: Principles and Applications, 2nd Edition*, Wiley-VCH, Weinheim, **2013**, p. 592; b) T. Chu, J. Xu, *J. Mol. Model.* **2016**, *22*, 200; c) V. S. Padalkar, S. Seki, *Chem. Soc. Rev*. **2016**, *45*, 169-202.

[8] a) Y. Ge, D. F. O'Shea, *Chem. Soc. Rev*., **2016**, *45*, 3846-3864; b) R. P. Tayade, N. Sekar, *J. Fluoresc*. **2017**, *27*, 167–180; c) B. Carlotti, E. Benassi, V. Barone, A. Spalletti. F. Elisei, *ChemPhysChem*. **2015**, *16*, 1440-1450; d) B. Carlotti, E. Benassi, C. G. Fortuno, V. Barone, A. Cesaretti, C. G. Fortuna, A. Spaletti, V. Barone, F. Elisei, *ChemPhysChem*. **2016**, *17*, 136-1446; e) E. Benassi, B. Carlotti, M. Segado, A. Cesaretti, A. Spalletti, F. Elisei, V. Barone, *J. Phis. Chem*. *B*. **2015**, *119*, 6035-6040; f) E. Benassi, F. Edigi, V. Barone, *J Phys. Chem*. **2015**, *119*, 3155-3173; g) K. Chen, H-Y. Tsai, *Int. J. Mol. Sci.* **2014**, *15*, 18706-18724; h) S. S. Razi, P. Srivastava, R. Ali, R. C. Gupta, S. K. Dwivedi, A. Mistra, *Sensor and Activators B: Chemical*. **2015**, *209*, 162-171.

[9] a) H. B. Jalani, A. N. Pandya, D. H. Pandaya, J. A. Sharma, V. Sudarsanam, K. K. Vasu, *Tetrahedron Lett*. **2012**, *53*, 6927-6930; b) N. P. Belskaya, K. I. Lugovik, A. D. Ivina, V. A. Bakulev, Z. J. Fan, *Chem. Het. Comp*. **2014**, *50*, 888-900.

[10] a) S. Tanaka, K. Ashida, G. Tatsuta, A. Mori, *Synlett* **2015**, *26*, 1496-1500; b) Y. Wang, M.-Y. Yang, M.-H. Zheng, X.-L. Zhao, Y.-Z. Xie, J.-Y. Jin, *Tetrahedron Lett.* **2016**, *57*, 2399-2402.

[11] a) R. F. W. Bader, H. Essen, *J. Chem. Phys*. **1983**, *80*, 1943-1960; b) R. F. W. Bader, Atoms in molecules. A quantum theory. Oxford: Oxford University Press; 1990. c) R. F. W. Bader, *Chem. Rev*. **1991**, *91*, 893-892.

[12] a) H. J. Bohórquez, C. F. Matta, R. J. Boyd, *Int. J. Quant. Chem*. **2010**, *110*, 2418-2425; b) E. R. Johnson, S. Keinan, P. Mori-Sánchez, J. Contreras-Garcia, A. J. Cohen, W. Yang, *J. Am. Chem. Soc*. **2010**, *132*, 6498-6506; c) *J. Lane, J. Contreras-García, J.-P. Piquemal, B. J. Miller, H. G. Kjaergaard, J. Chem. Theory Comput.* **2013**, *9*, 3263–3266; d) R. A. Boto, J. Contreras-Garcia, J. Tierny, J.-P. Piquemal, *Mol. Phys*. **2015**, DOI: 10.1080/00268976.2015.1123777; e) J. Andres, S. Berski, J. Contreras-Garcia, P. Gonzalez-Navarrete, *J. Phys. Chem*. **2014**, *118*, 1663-1672; f) *J. González, I. Baños, I. León, J. Contreras-García, E. J. Cocinero, A. Lesarri, J. A. Fernández, J. Millán J. Chem. Theory Comput.* **2016**, *12*, 523–534; g) Y. Zhang, H. He, K. Dong, S. Zhang, *RSC Adv.*, **2017**, *7*, 12670-12682.

[13] W. H. Melhuish, *J. Phys. Chem.* **1961**, *65*, 229-235.

[14] U. Schmidt, H. Kubitzek, *Chem. Ber.* **1960**, *93*, 1559-1564.

[15] M. Ruiz-Lopez in *Quantum Modeling of Complex Molecular Systems* (Ed.: J.-L. Rivail), Springer, Berlin, **2015**, pp. 343-365.

WILEY-VCH

FULL PAPER

**Entry for the Table of Contents** (Please choose one layout)

Layout 1:

## FULL PAPER

Text for Table of Contents

((Insert TOC Graphic here: max. width: 5.5 cm; max. height: 5.0 cm; NOTE: the final letter height should not be less than 2 mm.))

**Key Topic***

*Author(s), Corresponding Author(s)**

***Page No. – Page No.***

**Title**

*one or two words that highlight the emphasis of the paper or the field of the study

Layout 2:

## FULL PAPER

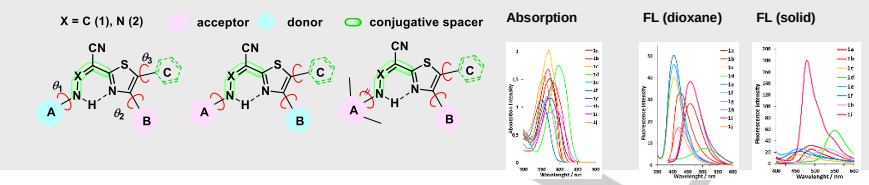


Two series of di- and trisubstituted thiazoles bearing pendant aryl enamine/aza-enamine groups (X = C, N) were synthesized, and their structural features, geometries and photophysical properties in solution and in the solid state were evaluated by spectroscopic methods and quantum mechanical calculations. The effect of weak intramolecular interactions on their photophysical properties was elucidated.

**Fluorescence, Intramolecular Charge Transfer***

*Kseniya I. Lugovik, Aleksandra V. Popova, Alexander K. Eltyshev, Enrico Benassi,* Nataliya P. Belskaya**

***Page No. – Page No.***

**Synthesis of Thiazoles Bearing Aryl Enamine/Aza-enamine Side Chains. Effect of the π-Conjugated Spacer Structure and Hydrogen Bonding on Photophysical Properties**